Electronic Supplementary Material (ESI) for Analyst.

Supporting information

Covalent-coordination tandem functionalization of metal-organic framework (UiO-66) as a hybrid probe for luminescence detection of trans, trans-muconic acid as a biomarker of benzene and Fe^{3+}

Jie Min[a], Xiang-Long Qu[a] and Bing Yan*[a,b]

[a] School of Chemical Science and Engineering, Tongji University, Siping Road 1239, Shanghai 200092, China.
[b] School of Materials Science and Engineering, Liaocheng University, Liaocheng 252059, China

E-mail: byan@tongji.edu.cn.

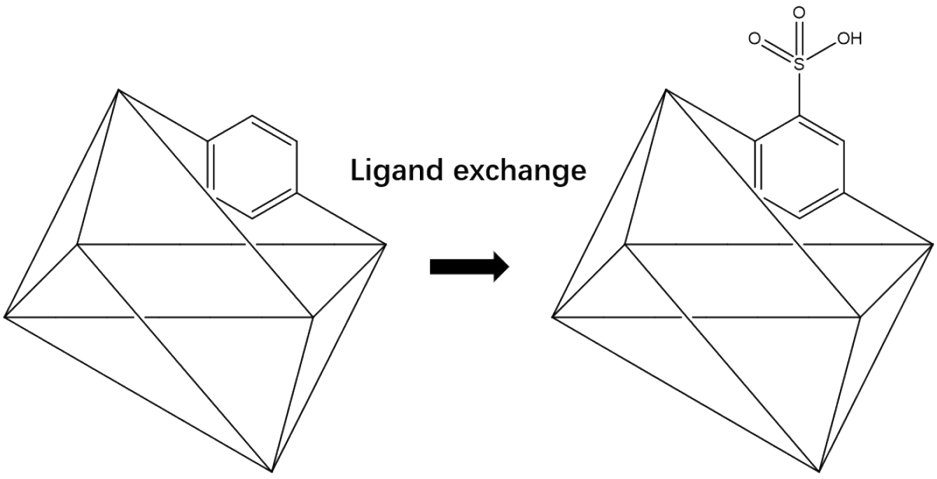

Figure S1 Synthetic route of UiO-66-SO_3H based on ligand exchange.

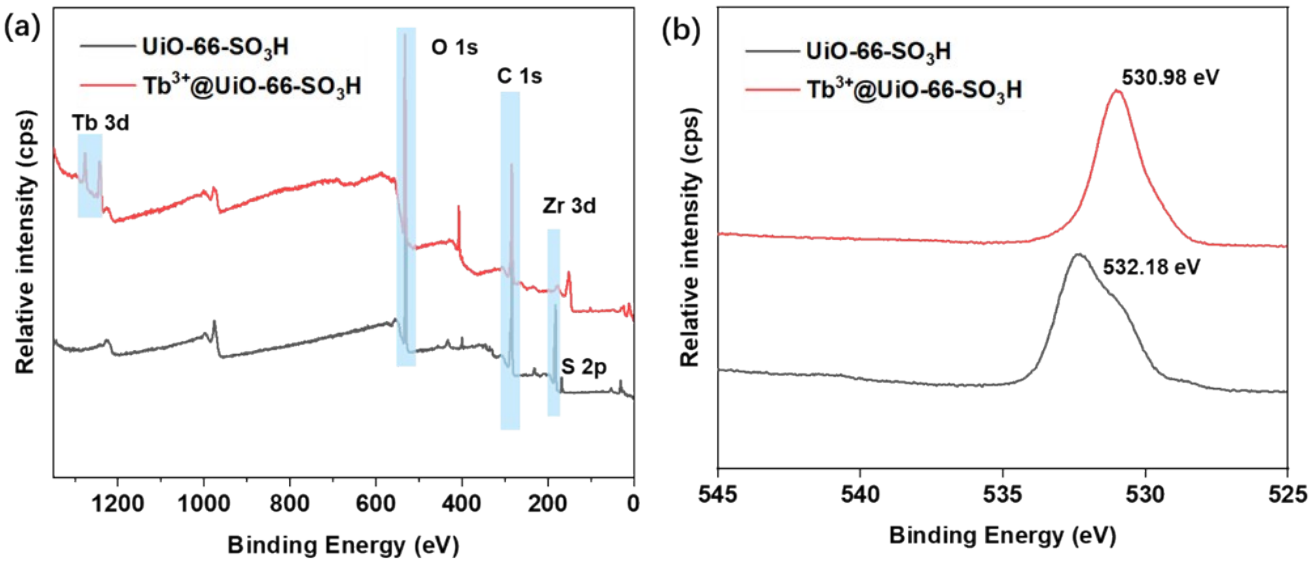

Figure S2 (a) Full XPS profiles for solid-state Tb^{3+}@UiO-66-SO_3H and UiO-66-SO_3H; (b) O 1s XPS patterns for solid-state Tb^{3+}@UiO-66-SO_3H and UiO-66-SO_3H.

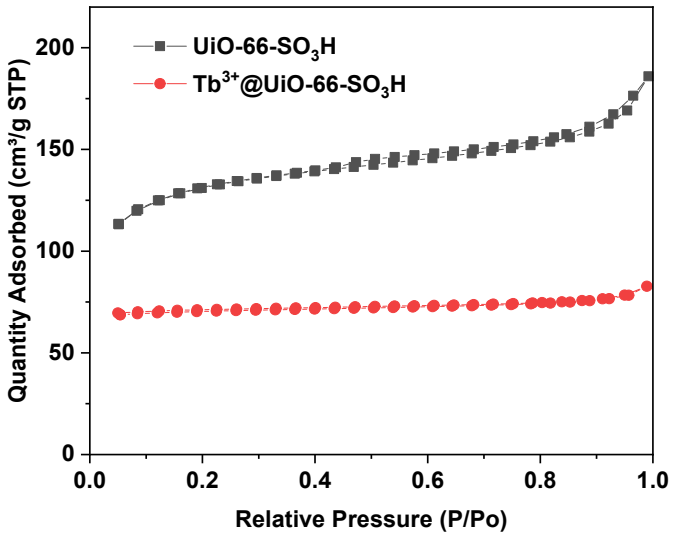

Figure S3 N_2 adsorption-desorption isotherms of solid-state Tb^{3+}@UiO-66-SO_3H and UiO-66-SO_3H.

Table 1 (a) Comparison of tt-MA detection between this work and some previously reports

Compound	Zr (ppm)	Tb (ppm)	Molar Ratio
Tb^{3+}@UiO-66-SO_3H	73.46	4.59	Zr/Tb 27.92/1

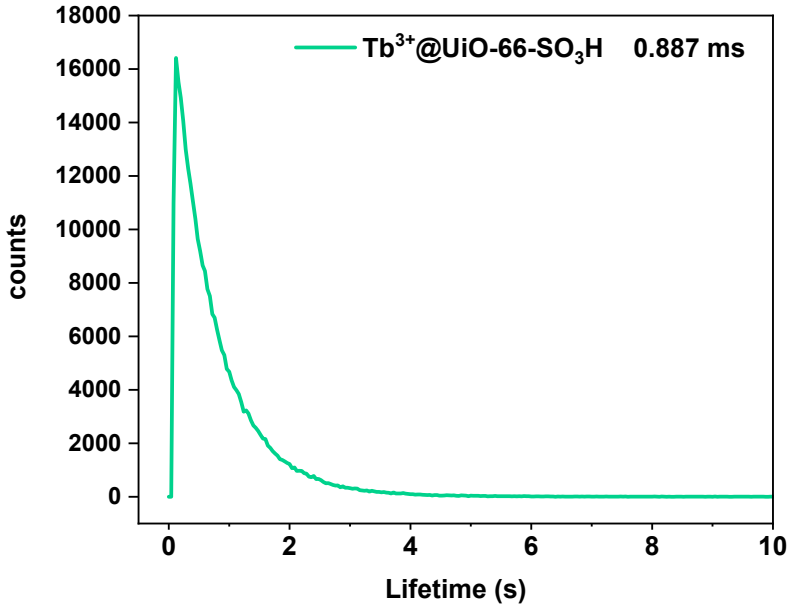

Figure S4 Emission decay profile of $^5D_4 \rightarrow {}^7F_5$ Tb^{3+} in Tb^{3+}@ UiO-66-SO_3H. (λ_{ex}= 301 nm)

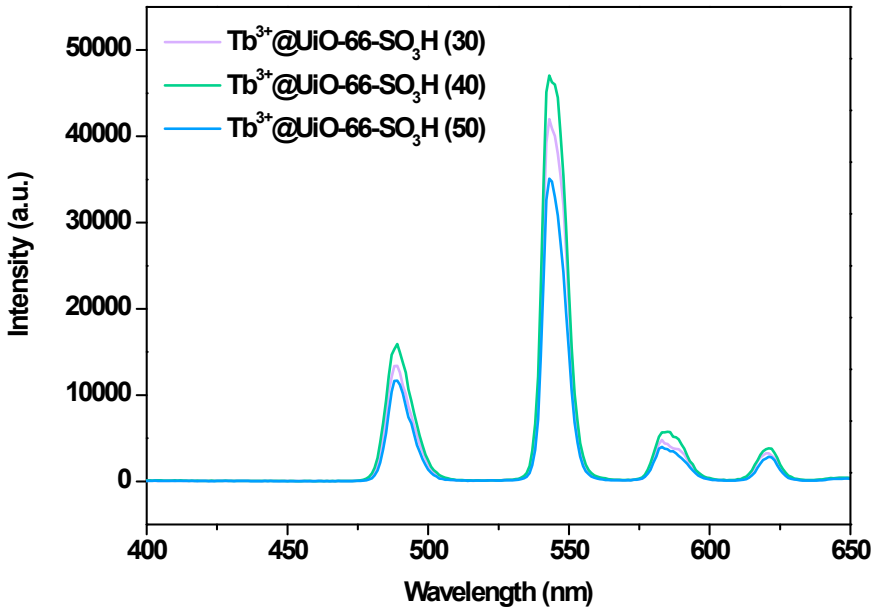

Figure S5 Emission spectra of solid-state Tb^{3+}@UiO-66-SO_3H with different molar content of sulfonic groups in ligands.

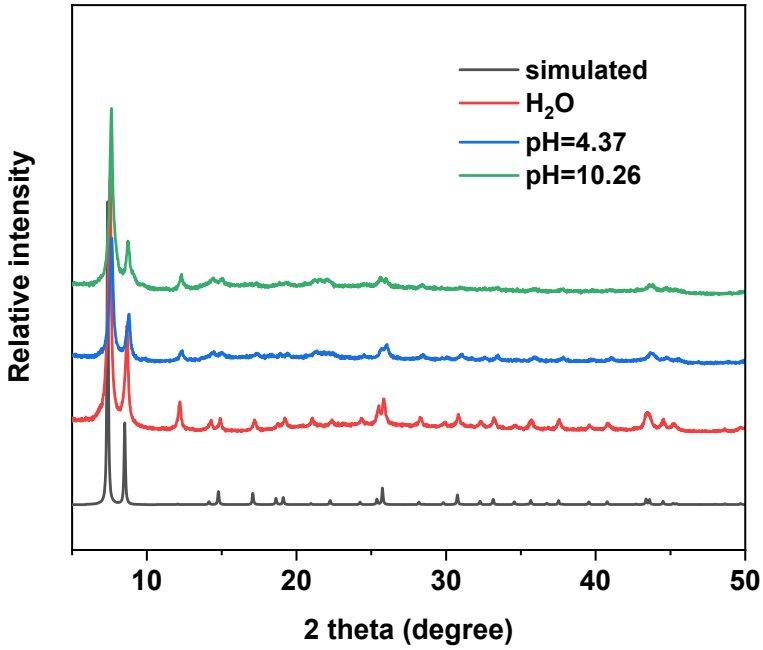

Figure S6 PXRD patterns of solid-state Tb^{3+}@ UiO-66-SO_3H collected from water, and aqueous solution with different pH values after immersion for 24 h.

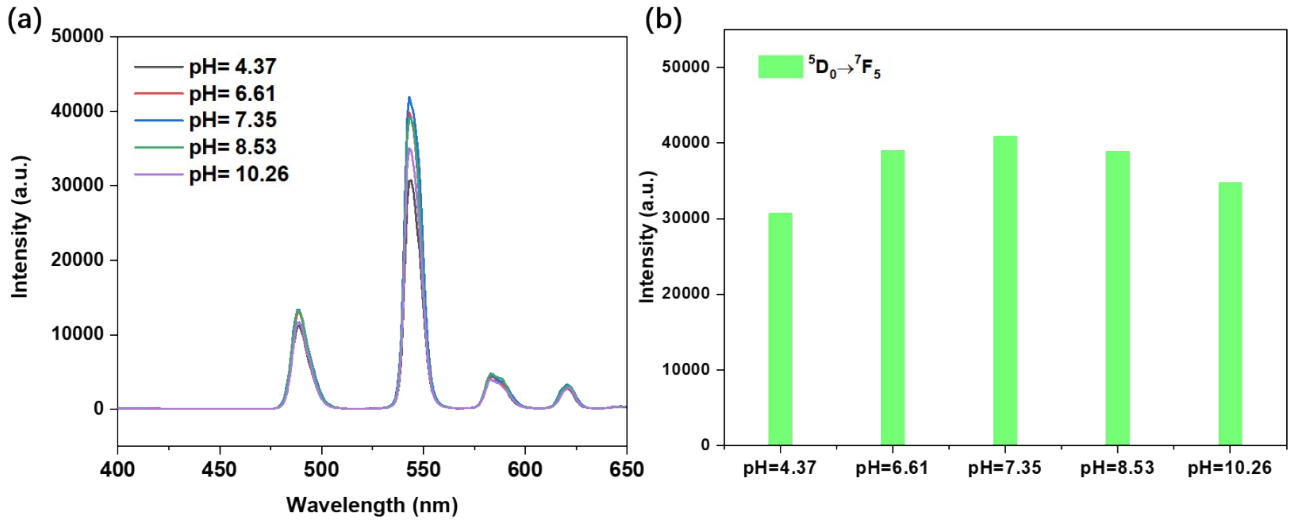

Figure S7 (a) Emission spectra of Tb^{3+}@ UiO-66-SO_3H in aqueous media with various pH values; (b) Corresponding emission intensity at 543 nm.

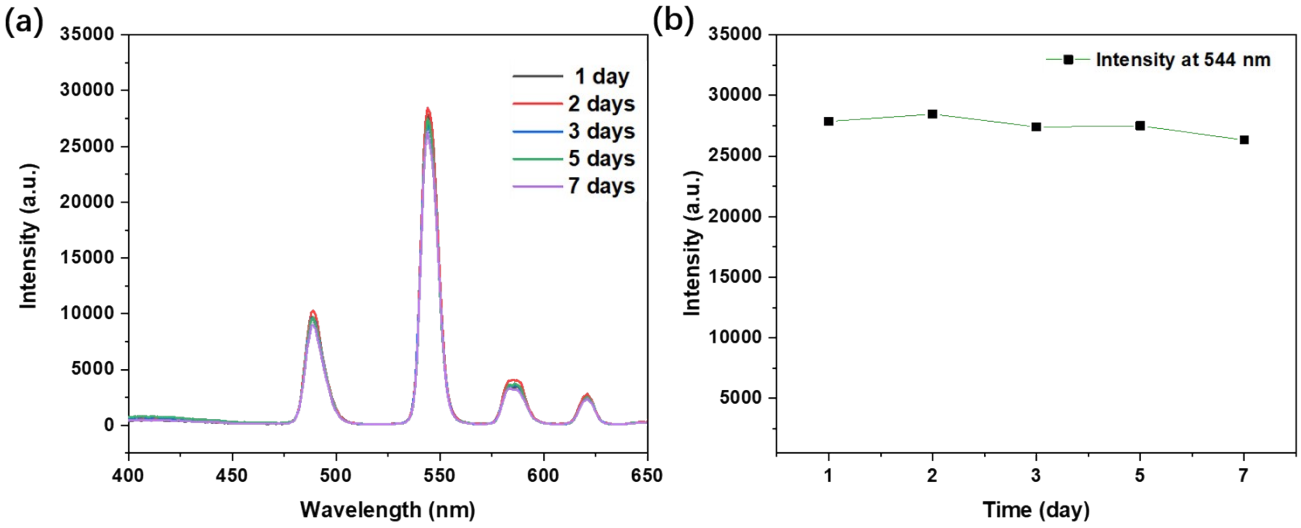

Figure S8 (a) Day-to-day fluorescence stability of Tb^{3+}@ UiO-66-SO_3H suspension under excitation at 301 nm; (b) Corresponding variation of emission intensity at 543 nm with time.

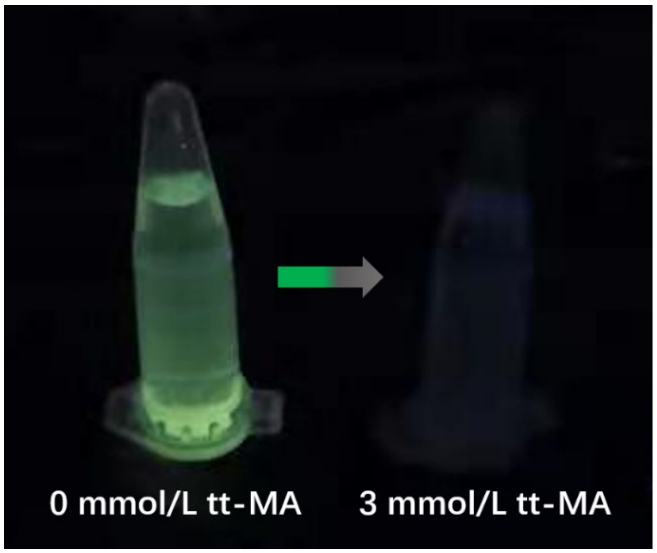

Figure S9 Photograph of Tb^{3+}@ UiO-66-SO_3H in aqueous solutions without tt-MA (left) and with 3 mmol/L tt-MA (right).

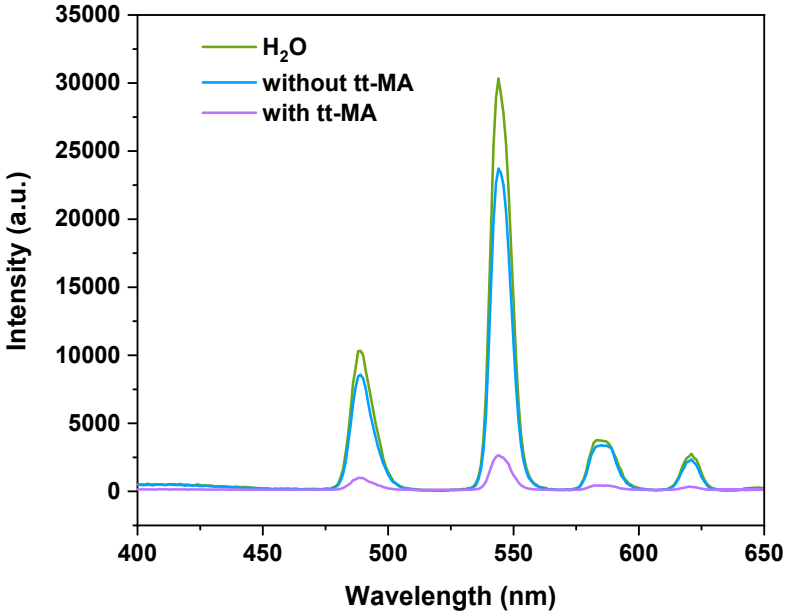

Figure S10 Emission profiles of Tb^{3+}@ UiO-66-SO_3H in pure water, artificial urine with and without 3 mmol/L of tt-MA.

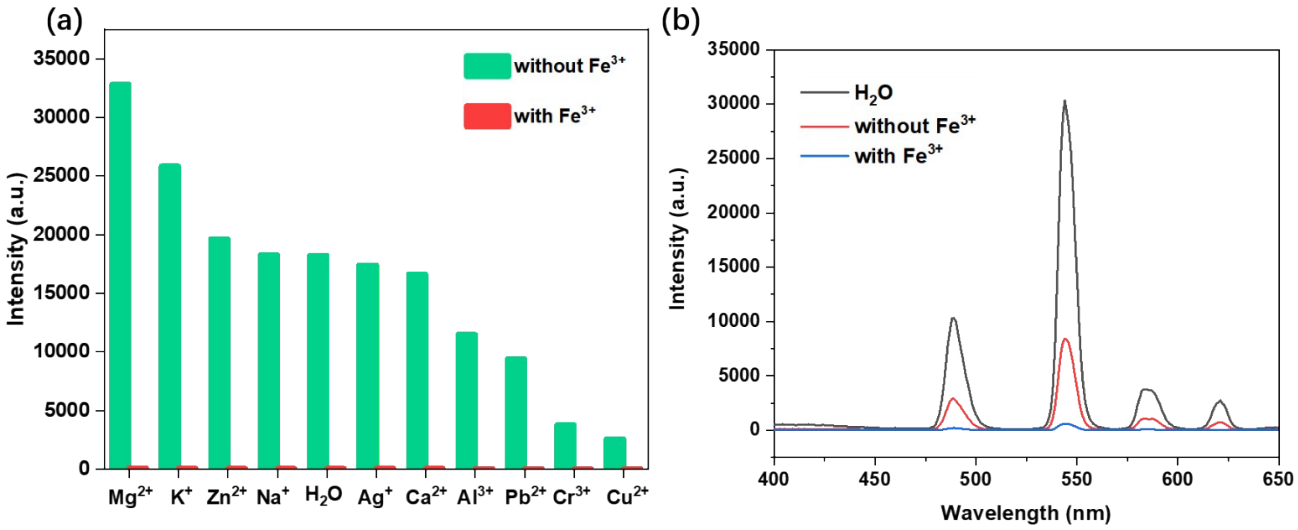

Figure S11 (a) Emission intensity of Tb^{3+}@UiO-66-SO_3H at 543 nm in different aqueous solutions of metal ions (10 mM) with and without Fe^{3+}. (λ_{ex}= 301 nm); (b) Emission profiles of Tb^{3+}@ UiO-66-SO_3H in pure water, solutions of various metals ions together with and without 3 mmol/L of Fe^{3+}.

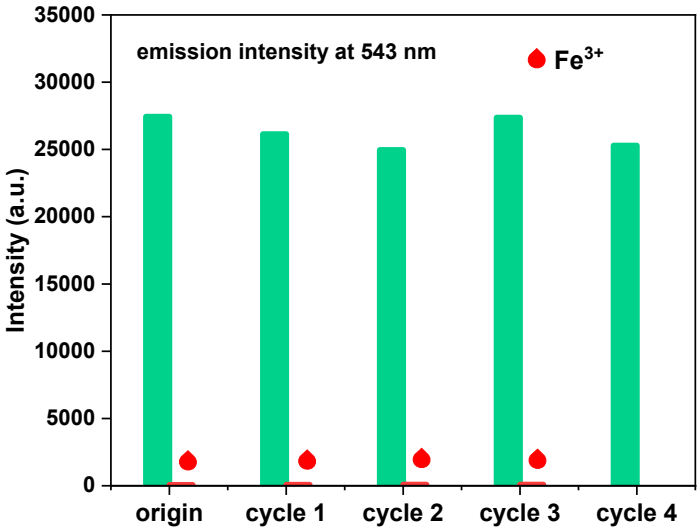

Figure S12 Emission intensity of Tb^{3+}@UiO-66-SO_3H at 543 nm after four recyclable sensing experiments for Fe^{3+}.

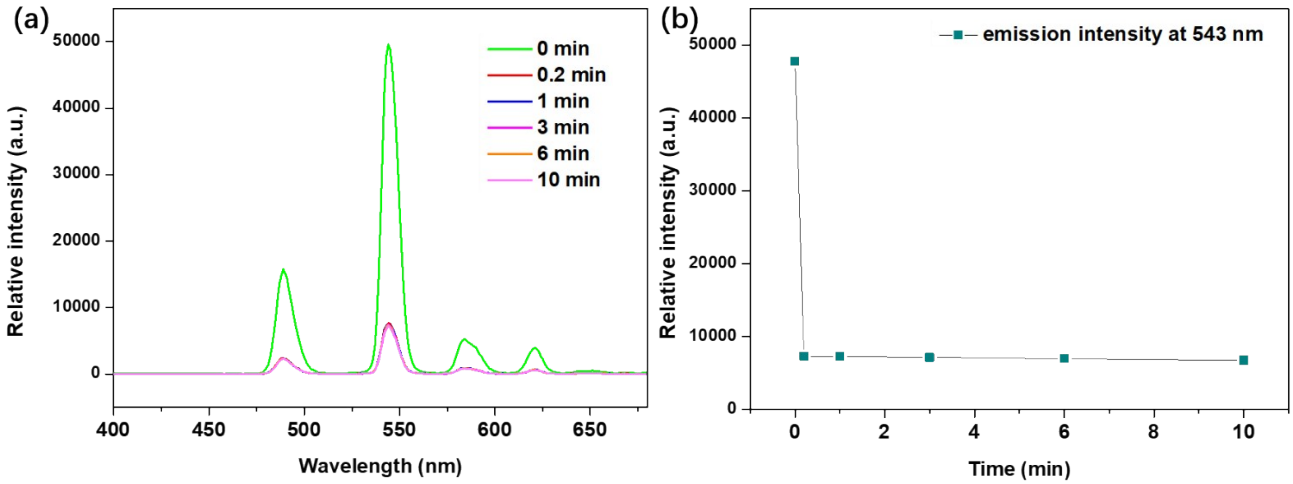

Figure S13 (a) Emission spectra of Tb^{3+}@ UiO-66-SO_3H with different immersion times in aqueous solution of Fe^{3+} (0.05 mM) under an excitation wavelength of 301 nm; (b) Variation of luminescent intensity of Tb^{3+}@ UiO-66-SO_3H at 543 nm with different immersion times.

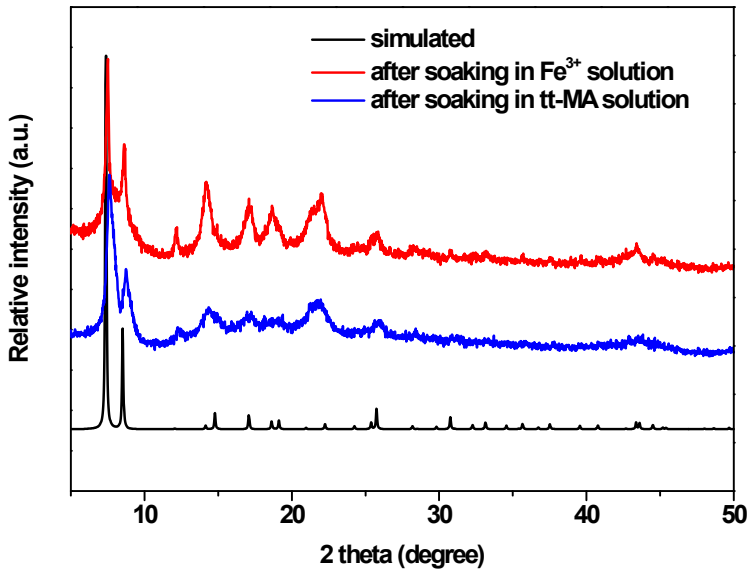

Figure S14 PXRD patterns of solid-state Tb^{3+}@ UiO-66-SO_3H after respectively soaking in the aqueous solutions of tt-MA and Fe^{3+} for 24 h.

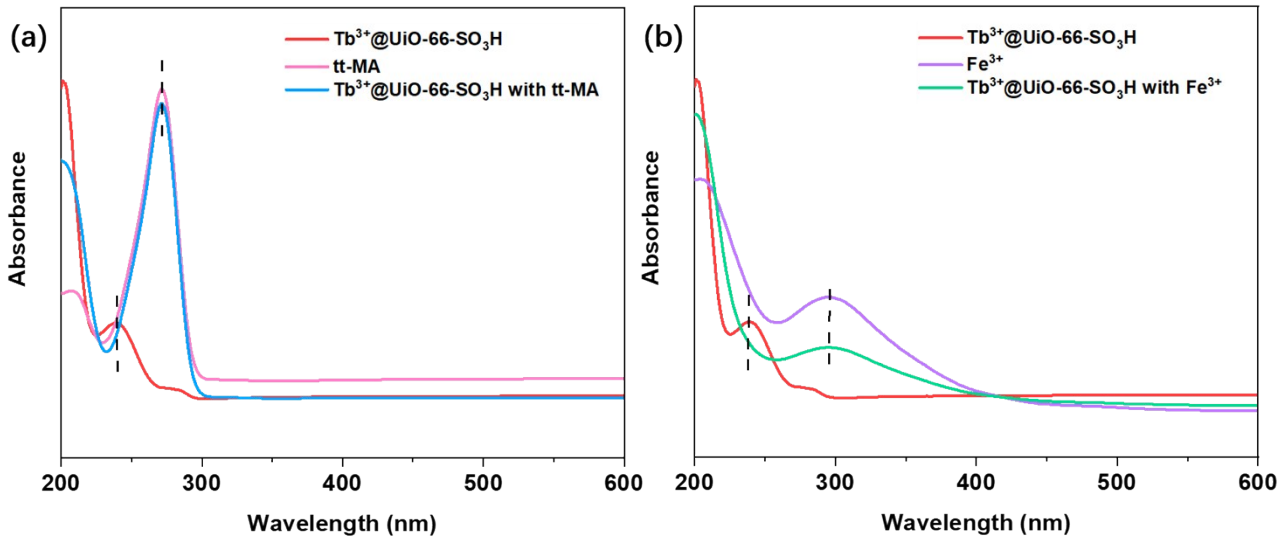

Figure S15 (a) UV-vis adsorption spectra of the aqueous suspensions containing Tb^{3+}@ UiO-66-SO_3H, tt-MA respectively, and containing both; (b) UV-vis adsorption spectra of the aqueous suspensions containing Tb^{3+}@ UiO-66-SO_3H, Fe^{3+} respectively, and containing both.

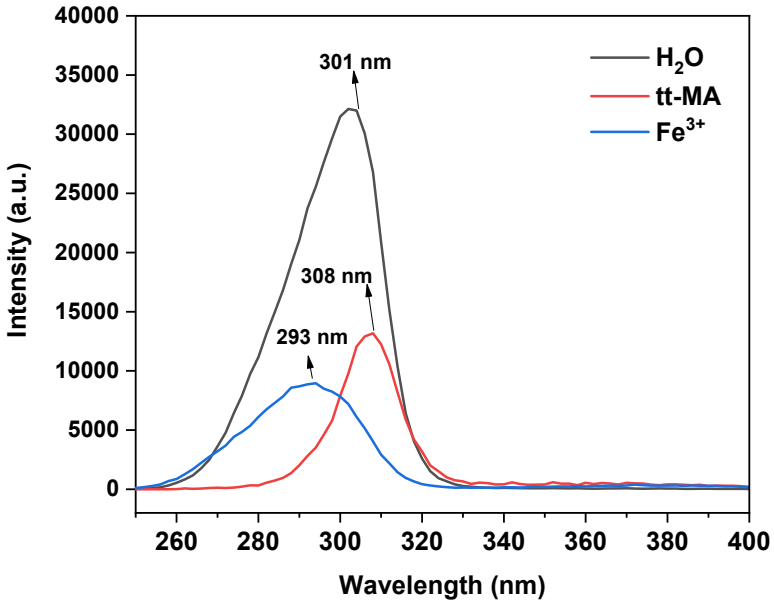

Figure S16 Excitation spectra of Tb^{3+}@ UiO-66-SO_3H in water, aqueous media with tt-MA and with Fe^{3+} separately at the maximum emission wavelength of 543 nm.

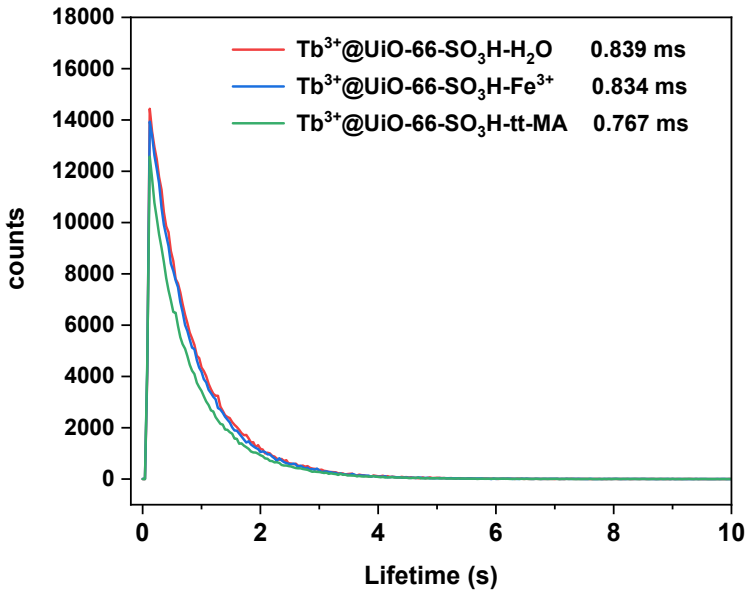

Figure S17 Emission decay profiles of $^5D_4 \rightarrow {}^7F_5$ Tb^{3+} in Tb^{3+}@ UiO-66-SO_3H in water, aqueous media with tt-MA and with Fe^{3+} separately.